International Journal of Hyperthermia

ISSN: 0265-6736 (Print) 1464-5157 (Online) Journal homepage: informahealthcare.com/journals/ihyt20

On the optimal choice of the exposure conditions and the nanoparticle features in magnetic nanoparticle hyperthermia

Gennaro Bellizzi & Ovidio M. Bucci

To cite this article: Gennaro Bellizzi & Ovidio M. Bucci (2010) On the optimal choice of the exposure conditions and the nanoparticle features in magnetic nanoparticle hyperthermia, International Journal of Hyperthermia, 26:4, 389-403, DOI: 10.3109/02656730903514685

To link to this article: https://doi.org/10.3109/02656730903514685

Published online: 08 Mar 2010.

Int. J. Hyperthermia, June 2010; 26(4): 389–403

informa
healthcare

On the optimal choice of the exposure conditions and the nanoparticle features in magnetic nanoparticle hyperthermia

GENNARO BELLIZZI[1] & OVIDIO M. BUCCI[1,2]

[1]*Dipartimento di Ingegneria Biomedica, Elettronica e delle Telecomunicazioni Università di Napoli Federico II, Napoli, Italia and* [2]*Istituto per il Rilevamento Elettromagnetico dell'Ambiente, Consiglio Nazionale delle Ricerche, Napoli, Italia*

(Received 29 September 2009; Revised 16 November 2009; Accepted 27 November 2009)

Abstract
Purpose: Two points are particularly relevant for the clinical use of magnetic nanoparticle hyperthermia: the optimisation of both the exposure conditions and the magnetic nanoparticle characteristics, and the assessment of the limits of scalability of the treatment. To answer these two points a criterion for the individuation of the magnetic field parameters and of the magnetic nanoparticle features that minimise the therapeutic concentration of nanoparticles to be used in magnetic nanoparticle hyperthermia is developed.
Methods: The proposed criterion is based on the estimation of the levels of heat generation rate, due to the electromagnetic field, to be supplied to both the cancerous and the neighbouring healthy tissues for achieving the therapeutic heating of the tumour with a desired degree of spatial selectivity. These quantities are determined by exploiting the Pennes bioheat transfer model.
Results: The reliability of the criterion has been proven by means of an extensive numerical analysis, performed by considering tumours of spherical shape embedded in tissues of cylindrical shape. Several cases, including tumours of different sizes and position have been considered.
Conclusions: By exploiting the proposed criterion a study of the clinical scalability of the therapeutic approach is presented.

Keywords: *hyperthermia, magnetic nanoparticles, electromagnetic fields, bioheat transfer equation, optimisation criteria*

Introduction

Hyperthermia is a form of anticancer therapy consisting in heating the cancerous tissue above a therapeutic temperature [1–7]. It is, indeed, well established that it is possible to induce damage or necrosis of cancerous cells by elevating their temperature above 42–48°C and maintaining it for approximately thirty minutes [1, 7]. Hyperthermia also increases the sensitivity of the cancerous cells to some therapeutic agents such as ionising radiations and certain cytotoxic drugs [2, 4, 7]. Thus, its combined use with radiotherapy and/or chemotherapy can significantly improve the efficacy of these anticancer treatments.

Among the modalities of anticancer hyperthermia till now proposed, magnetic nanoparticle hyperthermia (MNPH) [1–7] appears to be the most promising one, due to:

- the high capability of the magnetic nanoparticles (MNP) to convert into heat the energy of an applied, radio frequency (RF), magnetic field (MF) [8, 9];
- the possibility of selectively concentrating the MNPs at the cancer site by means of minimally invasive routes [10];
- the high transparency of the human tissues to RF MFs.

Indeed, thanks to these features, MNPH could enable the achievement of highly selective and homogeneous heating of the cancerous tissue, above the therapeutic temperature, even for deeply

Correspondence: Ovidio M. Bucci, Dipartimento di Ingegneria Biomedica, Elettronica e delle Telecomunicazioni Università di Napoli Federico II, via Claudio 21, 80125 Napoli, Italia. Tel: +39 081 5707999. Fax: +39 081 5705734. E-mail: bucci@unina.it

ISSN 0265–6736 print/ISSN 1464–5157 online
DOI: 10.3109/02656730903514685

sited tumours in the body otherwise unachievable by means of the other approaches. In addition, compared to systemic and regional hyperthermia MNPH has several advantages, because local heating can achieve higher temperatures, causes only limited patient discomfort [11, 12] and does not induce fever-like effects on the immune system [13].

Also, the recent development of MNPs with Curie temperature between 42° and 50°C [14] offers the unique opportunity of a self-regulated hyperthermia that would allow the problem of the generation of overheating within the irradiated tissues to be fully addressed [14], even though the biocompatibility of such MNPs is still to be investigated.

At present, two strictly related important aspects still need to be addressed in MNPH. The first concerns the optimisation of both the MNPs' heat generating properties and the MF parameters [5, 15]; the second is the estimation of the limits of clinical scalability of the treatment [15], namely the minimum tumour size and the maximum extension of the region of the body exposed to the applied field (irradiated tissues) which can be safely and effectively treatable.

Concerning the second point, the existence of these limits is essentially related to the maximum concentration of MNPs currently achievable in cancerous tissues, which, as is well known, is seriously limited by technical and biomedical restrictions. As a matter of fact, since the amount of MNPs required for a selective heating increases both when tumours of decreasing size are treated (in order to balance the higher capability of smaller tumours to dissipate heating towards the neighbouring tissues) and when the extension of the irradiated tissue grows (in order to compensate the larger amount of non-selective heating produced via Joule effect by the electric field), there exist a minimum tumour size and a maximum exposure region size, related to the maximum concentration of MNPs, beyond which cancer cannot be safely and successfully treated.

Although the assessment of the limits of scalability is a key point for the clinical applicability of MNPH, to the best of our knowledge, the experiences reported in literature mainly refer to in vitro tests [16, 17] or experiments performed on animals of small size [10, 18]. Despite promising results in animal models, few clinical trials on humans have been performed, mainly on an empirical basis, and only limited successes in treating cancer of the prostate [11, 12], brain [19] and different recurrent tumours [20] have been achieved. The poor results obtained in clinical trials proves that the scalability of the MNPH from animals to patients is not as trivial as one would hope, and requires a deeper description and theoretical characterisation of the interaction between the MNPs and the applied field, of the thermal flow from the heated site to the surrounding tissues and of the minimum size of the treatable tumours. Such a study has been previously attempted by Hergt and Dutz in [15]. Therein, by exploiting a simplified expression for the dependence of the temperature rise produced in the tumour on the MNP concentration, tumour size and specific absorption rate (SAR) of MNPs, together with experimental values of SAR, an estimate of the minimum tumour size successfully treatable is provided. The obtained result clearly highlights the difficulty of effectively treating malignancies smaller than about 10 mm in size and the impossibility of treating very small metastases disseminated in the body (less than 3 mm in size). However, apart from the simplified expression used for the temperature rise, the estimation performed by Hergt and Dutz [15] does not take into account the heating produced by the electric field (EF) in the tissues surrounding the tumour, although the experimental SAR used in the calculation has been measured by using MF amplitudes and frequencies large enough to induce a non-negligible EF. As a result, no estimation of the maximum size allowed for the irradiated region is given and an underestimate of the minimum tumour size effectively treatable is likely to be obtained.

Accordingly, for a reliable estimation of the actual limits of scalability of MNPH, an accurate description of the problem, taking into account the electric power dissipation within the irradiated tissues is mandatory. Obviously, this estimation can be correctly performed only once the best operative conditions, i.e. the optimal values of the MF amplitude and frequency, say H and f, as well as the optimal MNP size, say d, are identified.

Concerning this point, the optimal choice for H, f and d is, obviously, that maximising the SAR of the MNPs, i.e. that minimising the therapeutic concentration c of MNPs [21, 22], being the limits of scalability strictly related to the maximum c achievable in the tumour. Furthermore, the minimisation of c is desirable: (a) to limit the amount of magnetic material to be supplied and consequently to be expelled from the body after the treatment; (b) to make feasible the use of modalities of MNP delivery, such as the biochemical targeting, which are more efficient and selective than the intratumoural injection, but able to concentrate a smaller amount of MNPs at the cancer site [1].

However, the estimation of the optimal values for H, f and d is not an easy task, since at the same time it is required to limit the heating produced by the induced EF over the irradiated tissues, in order to preserve the integrity of the healthy tissue exposed to the applied field. For instance, SAR could be easily increased by increasing H and/or f, but unavoidably, this also increases the power dissipated, via Joule

effect, by the EF in the healthy tissues surrounding the tumour, with a subsequent reduction of the heating selectivity degree of the treatment (trade-off between dose minimisation and heating selectivity).

Likely, the above difficulty is the reason why in the literature, to the best of our knowledge, the choice of H, f and d is accomplished by using semi-empirical approaches. For instance, in Hergt and Dutz [15], by exploiting the models describing the dependence of the magnetic losses arising in MNPs on the MF parameters, guidelines for the optimal choice of H and f are given. However, to keep low the unwanted and non-selective heating produced in the healthy tissues by the EF, the product Hf is required to be about ten times larger than the safety threshold $4.85 \times 10^8\,\mathrm{A\,m^{-1}\,s^{-1}}$, which has been derived empirically by means of clinical trials on human volunteers [23].

Obviously, due to its empirical character, such a condition may either overestimate or underestimate the actual range of values of H and f exploitable in MNPH, leading in the first case to a non-safe treatment of the malignancy, and in the second case to the use of an over dosage of MNPs to balance the underestimate of the values of H and f.

The aim of the paper is to present a criterion for the optimal choice of the values of H, f and d, say H_o, f_o and d_o, to be used in MNPH.

The proposed approach determines H_o, f_o and d_o by estimating the mean specific heat generation rates, due to the magnetic and electric fields, p_m and p_e say, to be supplied to both the cancerous and the surrounding normal tissues for achieving the therapeutic heating of the tumour with a desired degree of heating selectivity. The values of p_m and p_e are determined by relating them to the steady-state temperature, say T, produced over the irradiated region by the applied field.

To describe the heat transfer mechanisms within the irradiated tissues the well known Pennes bioheat transfer equation (BHTE) [24] is exploited. Concerning this point, we wish to stress that we are aware of the discussions on the validity of the BHTE and the subsequent development of more accurate models for describing the contribution of the blood flow to the heat transfer in living tissues [24]. However, as established by many researchers, none of the proposed models can be generally applied to all types of tissues and organs [24]. Therefore, due to its relative simplicity and its proven suitability in predicting the temperature in several cases, the BHTE is still a widely used model to describe the heat transfer in living tissues [25–33] and thus it is the model adopted in this paper.

Once p_m and p_e have been evaluated, H_o, f_o and d_o are determined by exploiting the expressions relating them to p_m and p_e.

To prove the effectiveness of proposed approach, numerical results relative to tumours of spherical shape embedded in tissues of cylindrical shape are provided. These cases are of interest as they are representative of many practical situations such as tumours in arms, legs, torso, neck, etc.

Finally, by exploiting the proposed criterion, an estimate of the limits of scalability of MNPH is also provided.

Statement of the problem and basic assumptions

As briefly stated in the Introduction, the first step to estimate p_m and p_e is to relate them to the temperature rise, $T_\Delta = T - T_0$, produced in both the cancerous and neighbouring healthy tissues by the applied field, being T_0 the basal temperature of the human body, i.e. temperature produced by the metabolic activity under normal physiological conditions ($T_0 \approx 37^\circ\mathrm{C}$).

To describe the thermal balance within the regions of interest, the steady state linearised, BHTE [25] is exploited, namely:

$$\vec{\nabla}\cdot\left(k(\underline{r})\vec{\nabla}T_\Delta(\underline{r})\right) - c_b w_b(\underline{r})T_\Delta(\underline{r}) - c_b w_b(\underline{r})(T_0 - T_b) + \dot{q}_{met}(\underline{r}) + \dot{q}(\underline{r}) = 0 \quad (1)$$

where k is the thermal conductivity of the irradiated tissues ($[k] = \mathrm{W\,m^{-1\circ}C^{-1}}$), w_b the blood perfusion rate ($[w_b] = \mathrm{kg\,m^{-3}\,s^{-1}}$), c_b the specific heat capacity of blood ($[c_b] = \mathrm{J\,kg^{-1\circ}C^{-1}}$), T_b the temperature of blood, $\dot{q}_{met}$ the basal metabolic heat generation rate and $\dot{q}$ the specific heat generation rate due to the applied field ($[\dot{q}] = [\dot{q}_{met}] = \mathrm{W\,m^{-3}}$). The dependence on the position vector $\underline{r}$ ($[\underline{r}] = \mathrm{m}$) of the above quantities takes into account the non-spatial homogeneity of the thermal properties of the human tissues.

We use the steady state BHTE since, as stated in the Introduction, the temperature rise in the tumour must be kept for at least 30 min for the achievement of the desired therapeutic results.

Hereafter, the following reasonable assumptions will be made:

(1) $T_b = T_0$;
(2) The MF produced by the exposure apparatus is essentially constant over the diseased area;
(3) A uniform temperature, $T = T_{\mathrm{ext}}$, is kept at the boundary of the irradiated region [29].

Assumption 1 is quite natural [25–32]. Assumption 2 is surely satisfied in practice, due to the relative smallness of the malignancies of interest. Assumption 3 is consistent with the use of thermostatic baths arranged around the irradiated region to

limit the temperature rise produced by the EF in the healthy tissues.

According to above assumptions, the thermal problem to be solved consists of Equation 1 with $T_b = T_0$ and the following boundary condition and specific heat generation rate:

$$T_\Delta(\underline{r})\big|_{\partial V} = T_{ext} - T_0 = \Delta T_{ext} \tag{2a}$$

$$\dot{q}(\underline{r}) = \dot{q}_m(\underline{r}) + \dot{q}_e(\underline{r}) = p_m x(\underline{r}) + p_e e^2(\underline{r}) \tag{2b}$$

In Equations 2a and 2b ∂V denotes the boundary of the irradiated region (V is the volume of the irradiated region), $\dot{q}_m$ the specific heat generation rate (power density) induced by the MF in the cancerous tissue, due to the presence of the MNPs, and $\dot{q}_e$ the power density induced by the EF over the irradiated region due to the non-null electric conductivity of the biological tissues.

Also, the quantities of interest p_m and p_e appearing in Equation 2b are defined as:

$$p_m = \frac{1}{V_1}\int_{V_1} \dot{q}_m(\underline{r})\mathrm{d}v \tag{3a}$$

$$p_e = \frac{1}{V}\int_{V} \dot{q}_e(\underline{r})\mathrm{d}v \tag{3b}$$

where V_1 denotes the volume of the diseased region, $x(\underline{r})$ is a function describing the spatial distribution of MNPs in the tumour (this function is assumed equal to zero outside the tumour), while $e(\underline{r})$ is a function taking into account the non-spatial uniformity of both the EF and the electric properties of the irradiated region.

For the linearity of the problem, the steady-state temperature T can be expressed as follows:

$$\begin{aligned} T(\underline{r}) = T_\Delta(\underline{r}) + T_0 = p_m f_m(\underline{r}) + p_e f_e(\underline{r}) \\ + p_{met} f_{met}(\underline{r}) + \Delta T_{ext} f_{ext}(\underline{r}) + T_0 \end{aligned} \tag{4}$$

In Equation 4 p_{met} is the mean value, calculated over the irradiated volume V, of $\dot{q}_{met}$ (i.e, Equation 3b with $\dot{q}_{met}$ in place of $\dot{q}_e$), $f_m(\underline{r})$, $f_e(\underline{r})$ and $f_{met}(\underline{r})$ are the solutions of the above thermal problem with $\Delta T_{\mathrm{ext}} = 0^\circ\mathrm{C}$ and $(p_m, p_e, p_{met}) = (1, 0, 0)\,\mathrm{W\,m^{-3}}$, $(p_m, p_e, p_{met}) = (0, 1, 0)\,\mathrm{W\,m^{-3}}$ and $(p_m, p_e, p_{met}) = (0, 0, 1)\,\mathrm{W\,m^{-3}}$, respectively, while $f_{ext}(\underline{r})$ is the solution of the problem with $\Delta T_{\mathrm{ext}} = 1^\circ\mathrm{C}$ and $(p_m, p_e, p_{met}) = (0, 0, 0)\,\mathrm{W\,m^{-3}}$. Equation 4 is the relation we will use in the following to estimate p_m and p_e from the desired temperature requirements.

It is worth noting that, unlike p_m and p_e, $f_m(\underline{r})$, $f_e(\underline{r})$, $f_{met}(\underline{r})$ and $f_{ext}(\underline{r})$ are known once the physiological, thermal and electromagnetic features of the irradiated region, the spatial distribution of MNPs in the tumour, and the applied field are known. Their expression can be obtained either in analytical form, if a canonical geometry for the irradiated tissues and the applied field is assumed, or, more generally, in a numerical way, by using proper computational tools.

As a final remark, let us note that the hypothesis of linearity assumed for the thermal model requires that the dependence on T of k, c_b, w_b and $\dot{q}_{met}$ can be neglected. However, in the case of w_b this assumption disagrees with the experimental observations which, on the contrary, show a remarkable dependence on T within the temperature range of interest in hyperthermia (42–48°C) [30–32], due to the action of the thermoregulatory system of the human body. In particular, a Gaussian profile, centred around 45°C, has been found for the temperature dependence of w_b in normal tissues, with a peak value even nine times larger than the basal one for muscles, while a step-like profile, dropping at about 42°C, has been found for the temperature dependence of w_b in cancerous tissues [30–32]. Accordingly, a linear model could appear unsuited to a reliable prediction of the temperature rise over the irradiated tissues. However, as will be shown in the next sections, the proposed criterion determines p_m and p_e by requiring that the produced temperature field T is never larger than a safety value, here set equal to 39°C, all over the irradiated healthy tissue. For this temperature rise a not significant increase of the blood perfusion rate in normal tissues is observed [30–32, 34] so that a constant value for w_b in the healthy tissue can be confidently assumed. On the contrary, for the tumoural tissue, where a temperature larger than 42°C is required, the dependence on T of w_b should be considered. However, the very small dimension of the tumour, as compared to the surrounding tissue, and the non-strong dependence on T of w_b make the assumption of linearity not critical, so that a constant value for w_b can be again retained, without appreciably trusting the confidence of the numerical estimates. In light of the above considerations and taking into account the unavoidable inaccuracies due to the variability of the electromagnetic and thermal parameters of the tissues, the adoption of a linear model appears quite justified.

Criterion for estimating p_m and p_e

As recalled before, in MNPH the therapeutic heating of the tumour should be as selective as possible, i.e. should involve as much as possible only the malignant tissue, in order to preserve the integrity of the surrounding normal tissue. Ideally, a temperature distribution where all the diseased area is above the therapeutic temperature, T_1, and all the surrounding healthy tissue is at $T = T_0$ should be attained. However, due to the non-null thermal conductivity of the biological tissues and the heating generated by

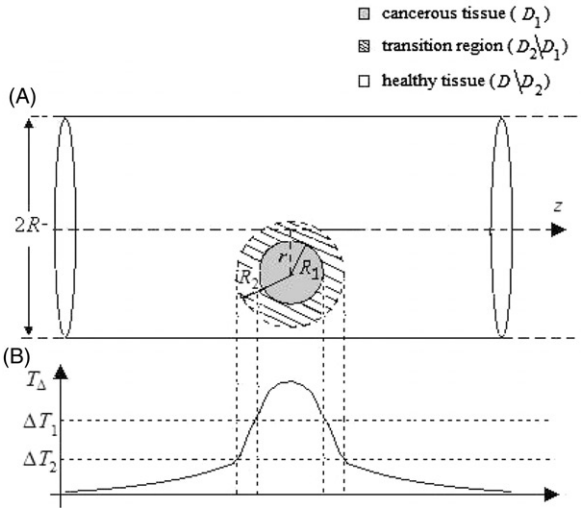

Figure 1. (a) Geometry assumed for the tumour (grey region) and for the irradiated surrounding tissue (white region). The dashed circle, with radius R_2, represents the transition region surrounding the tumour; (b) a sketch of the actual profile expected for the temperature rise after MNPH treatment.

the unavoidable presence of the EF in the healthy tissue, the actual profile of temperature achievable in MNPH is always characterised by a non uniform value in the tumour and a non null transition region, surrounding the tumour, wherein T decreases from T_1 to a smaller, safety, value T_2 (see Figure 1b). Accordingly, p_m and p_e should be determined by requiring that T is as close as possible to the ideal temperature profile [26].

As a matter of fact, although a uniform temperature in the tumour is desirable, in order to have the same therapeutic conditions over all the diseased area, more important is to reduce the transition region width in order to increase the heating selectivity of the treatment. Therefore, p_m and p_e can be determined by requiring that the transition region has a given width, representing the desired degree of heating selectivity. This is the basic idea of the criterion proposed here to estimate the values of p_m and p_e.

Denoting with D the whole irradiated region and with D_1 the diseased region, containing the MNPs, and considering a third region, D_2, containing D_1 and enclosed in D, p_m and p_e are determined by requiring that the temperature rise T_Δ is larger than the therapeutic value, $\Delta T_1 = T_1 - T_0$, all over D_1 and smaller than a safety value, $\Delta T_2 = T_2 - T_0$ outside D_2, where ΔT_1, ΔT_2 and the width of D_2 represent the desired degree of hyperthermia and heating selectivity, respectively (see Figure 1a). In other words, the criterion estimates p_m and p_e by requiring that:

$$T_\Delta(\underline{r}') = p_m f_m(\underline{r}') + p_e f_e(\underline{r}') + p_{met} f_{met}(\underline{r}') + \Delta T_{ext} f_{ext}(\underline{r}') \geq \Delta T_1 \quad (\underline{r}' \in D_1) \tag{5a}$$

$$T_\Delta(\underline{r}'') = p_m f_m(\underline{r}'') + p_e f_e(\underline{r}'') + p_{met} f_{met}(\underline{r}'') + \Delta T_{ext} f_b(\underline{r}'') \leq \Delta T_2 \quad (\underline{r}'' \in D \backslash D_2) \tag{5b}$$

where $\underline{r}'$ and $\underline{r}''$ are the position vectors of a generic point belongs to D_1 and $D\backslash D_2$, respectively, $D\backslash D_2$ denoting the complement of D_2 with respect to D.

By solving Equations 5a and b one obtains for p_m and p_e the following inequalities:

$$p_m \geq \frac{\left\{ \begin{array}{l} \Delta T_1 f_e(\underline{r}'') - \Delta T_2 f_e(\underline{r}') + p_{met}(f_{met}(\underline{r}'') f_e(\underline{r}') \\ \quad - f_{met}(\underline{r}') f_e(\underline{r}'')) + \Delta T_{ext}(f_{ext}(\underline{r}'') f_e(\underline{r}') \\ \quad - f_{ext}(\underline{r}') f_e(\underline{r}'')) \end{array} \right\}}{f_m(\underline{r}') f_e(\underline{r}'') - f_m(\underline{r}'') f_e(\underline{r}')} = F_m(\underline{r}', \underline{r}'') \tag{6a}$$

$$p_e \leq \frac{\left\{ \begin{array}{l} \Delta T_2 f_m(\underline{r}') - \Delta T_1 f_m(\underline{r}'') + p_{met}(f_{met}(\underline{r}') f_m(\underline{r}'') \\ \quad - f_{met}(\underline{r}'') f_m(\underline{r}')) + \Delta T_{ext}(f_{ext}(\underline{r}') f_m(\underline{r}'') \\ \quad - f_{ext}(\underline{r}'') f_m(\underline{r}')) \end{array} \right\}}{f_m(\underline{r}') f_e(\underline{r}'') - f_m(\underline{r}'') f_e(\underline{r}')} = F_e(\underline{r}', \underline{r}'') \tag{6b}$$

where $(\underline{r}', \underline{r}'') \in D_1 \times (D\backslash D_2)$ and $\times$ as usual denotes the Cartesian product between sets.

Accordingly, to meet the therapeutic requirements of hyperthermia and heating selectivity, p_m and p_e must be chosen according to the following criterion[1]:

$$p_m \geq \max_{\underline{r}', \underline{r}'' \in D_1 \times (D\backslash D_2)} \{F_m(\underline{r}', \underline{r}'')\} \tag{7a}$$

$$p_e \leq \min_{\underline{r}', \underline{r}'' \in D_1 \times (D\backslash D_2)} \{F_e(\underline{r}', \underline{r}'')\} \tag{7.b}$$

It is worth noting that the right hand of Equation 7b can assume either positive or negative values, although p_e is a non-negative quantity. This incongruence occurs when the assigned requirements on the temperature rise, over the regions of interest, are not physically achievable. In this case weaker requirements should be reassigned.

As a concluding remark, we wish to stress that the described criterion is independent of the expressions of $f_m(\underline{r})$, $f_e(\underline{r})$, $f_{met}(\underline{r})$ and $f_{ext}(\underline{r})$, which depend on the adopted bioheat transfer model. Accordingly, the proposed criterion can be applied not only to the BHTE, as made in the present paper, but to any other bioheat transfer model, provided that linearity can be assumed.

In the next section the procedure to identify H_o, f_o and d_o from the knowledge of p_m and p_e, which completes the proposed criterion, will be described.

Optimal choice for *H*, *f*, *d*

To determine the optimal values for H, f and d, firstly one needs to relate them to p_m, p_e and c.

To this end, let us start by considering the expression of the electric power density dissipated over the irradiated region by the induced EF:

$$\dot{q}_e(\underline{r}) = \frac{\sigma_t(\underline{r})}{2}(E(\underline{r}))^2 \tag{8}$$

In Equation 8 $\sigma_t(\underline{r})$ is the electric conductivity of the irradiated tissues ($[\sigma_t] = \Omega^{-1}\,\mathrm{m}^{-1}$) and $E(\underline{r})$ is the EF amplitude.

Now, as long as inductive applicators (like coils) and sufficiently low frequencies are exploited, as happen in MNPH, according to the Faraday's law, a linear relation can be adopted between $E(\underline{r})$ and Hf:

$$E(\underline{r}) = (\mu_0 Hf)e'(\underline{r}) \tag{9}$$

where μ_0 is the free space permeability and $e'(\underline{r})$ a function taking into account the non-spatial uniformity of the EF.

By replacing Equation 9 in Equation 8 and averaging over the whole irradiated region, i.e. Equation 3b, one obtains the following relation among p_e, H and f:

$$p_e = \frac{(\mu_0 Hf)^2}{2}\left(\frac{1}{V}\int_V \sigma_t(\underline{r})(e'(\underline{r}))^2 \mathrm{d}v\right) = \frac{(\mu_0 Hf)^2}{2}\bar{\sigma}_t \tag{10}$$

where $\bar{\sigma}_t$ denotes the integral in brackets.

Accordingly, the determination of p_e allows the actual constraint on the product Hf exploitable in MNPH to be stated.

Concerning the dependence of p_m on H, f, d and c, one can exploit the models available in literature, describing the magnetic losses arising in MNPs when subjected to an applied RF MF [8, 9]. For an assembly of mono-disperse single domain MNPs suspended in a viscous environment, as happens in MNPH, different relations for p_m have been proposed depending on the nature of the loss mechanisms. For instance, if the relaxation losses are the main loss mechanisms, the following expression, in the small MF amplitude approximation, holds [8]:

$$p_m = c\frac{\pi(\pi\mu_0 M_s Hf)^2}{9k_b T}\frac{\tau_{eff}(d)d^3}{1+\left(2\pi f\tau_{eff}(d)\right)^2} \tag{11}$$

where M_s is the saturation magnetisation of each MNP, k_B the Boltzmann's constant, T the temperature (in degrees Kelvin) and τ_{eff} the effective relaxation time of the magnetisation decay of the MNPs.

In particular, $\tau_{\mathrm{eff}} = \tau_{\mathrm{N}}\tau_{\mathrm{B}}/(\tau_{\mathrm{N}}+\tau_{\mathrm{B}})$ where [8]:

$$\tau_N = \frac{\sqrt{\pi}}{2}\tau_0\sqrt{\frac{k_B T}{k_a \mathrm{v}_m}}\exp\left(\frac{k_a \mathrm{v}_m}{k_B T}\right) \tag{12a}$$

is the *Neel* relaxation time and [8]:

$$\tau_B = \frac{3\eta \mathrm{v}_H}{k_B T} \tag{12b}$$

is the *Brownian* relaxation time.

In Equations 12a and 12b, τ_0 is a characteristic time depending on the magnetic material composing the MNPs, k_a the effective anisotropy constant of the MNPs, v_m the volume of the magnetic core, v_H the hydrodynamic volume and η the effective viscosity of the medium containing the MNPs (i.e., cell plasma, cell membrane, extracellular matrix).

It is worth noting that the reliability of Equations 11, 12a and 12b in predicting p_m for suspensions of MNPs, has been assessed in several cases. For instance, one can refer to results in [35–37] where experimental values of SAR relative to iron oxide MNPs, measured by means of calorimetric approaches, have been shown to compare favourably with the estimates obtained by using Equations 11, 12a and 12b.

Alternatively, if the hysteresis losses are the dominant loss mechanisms, the following relation for p_m, experimentally verified by Hergt et al. [9], can be used:

$$p_m = c\left(4\mu_0 M_R H_c(d) f\left(1-\left(\frac{H_c(d)}{H}\right)^5\right)u(H-H_c(d)) + \alpha \mathrm{d} f H^3 u(H_c(d)-H)\right) \tag{13}$$

where M_R is the remanent magnetisation of the assembly of MNPs, α a parameter whose value depends on the type of MNPs [9], $u(\cdot)$ a step function equal to one for $H > H_c$, and $H_c(d)$ the coercivity field, given by:

$$H_c(d) = H_M(d/d_1)^{-0.6}\left[1-\exp\left(-(d/d_1)^5\right)\right] \tag{14}$$

being H_M and d_1 empirical parameters whose values depend again on the type of MNPs [9].

Later on, we will exploit, in turn, both Equations 11 and 13 for estimating H_o, f_o and d_o.

It is worth noting that, whatever the model adopted for the magnetic losses (i.e. Equations 11 or 13), p_m is proportional to c. Accordingly, given the MF and MNP characteristics, the estimation of p_m enables to know the actual dosage of MNPs to be used in the treatment.

At this stage it is possible to find H_o, f_o and d_o from the knowledge of p_m and p_e. In particular, denoted with p_{m0} and p_{e0} the values of p_m and p_e obtained from the criterion described in the previous section, the allowable values of c, H, f and d are those satisfying Equation 10 and one of Equations 11 or 13 (depending on the adopted model), with $p_m = p_{m0}$

and $p_e = p_{e0}$. Among these, the best choice for H, f and d is that with the smallest value of c.

As shown in Appendix A, if we adopt Equation 11 for p_m then $H_o = H_{\max}$, being $H_{\max}$ the maximum MF amplitude that the used exposure apparatus can produce. As a consequence, according to Equation 10, $f_o = (2p_e/\bar{\sigma}_t)^{1/2}(\mu_0 H_{\max})^{-1}$. Then, d_o is determined by maximising the right hand of Equation 11 with $p_m = p_{m0}$, $H = H_o$ and $f = f_o$ (see Appendix A).

On the other hand, if Equation 13 is exploited instead of Equation 11, then $H_o \approx 1.43 H_{c\max}$, where $H_{c\max}$ is the maximum value of the coercivity field $H_c(d)$, given by Equation 14 (see Appendix B). Consequently, $d_o \approx d_{\max}$, being $d_{\max}$ the MNP size at which $H_c(d)$ reaches the maximum (see Appendix B), and f_o is given by Equation 10 by setting $H = H_o \approx 1.43 H_{c\max}$. It is worth noting that if $H_{\max}$, is smaller than $1.43 H_{c\max}$, the best choice for the MF amplitude becomes $H_o = H_{\max}$. In this case, d_o is determined by the condition $1.43\ H_c(d) = H_{\max}$.

As a concluding remark, let us note that all the above considerations keep valid in the more realistic case of polydisperse MNPs, characterised by a lognormal distribution size $g_d(\rho|\mu_d, \sigma_d)$, being μ_d and σ_d the mean value and the standard deviation, respectively (see Appendixes A and B).

Numerical results

To test the reliability of the proposed criterion, an extensive numerical analysis has been performed by considering tumours of spherical shape embedded in normal tissues of cylindrical shape (see Figure 1A).

Several cases relative to tumours of different radius R_1, and radial positions r (see Figure 1A) as well as surrounding irradiated tissues of various extensions R have been examined. They are representative of many practical situations such as tumours in torso, arms, legs, neck, etc. Obviously, the values of R_1 and R have been chosen in agreement with the tumour sizes typically detectable by means of the conventional diagnostic techniques and with the typical dimensions of the aforementioned parts of the human body, respectively.

For the sake of simplicity, the analysis has been carried out by assuming electrically and thermally homogeneous tissues. In particular, the following values for k, c_b, w_b, p_{met} and σ_t have been adopted: $k = 0.6\,\mathrm{W\,m^{-1}{}^{\circ}C^{-1}}$, $c_b = 3.9\,\mathrm{kJ\,kg^{-1}{}^{\circ}C^{-1}}$ [38], $w_b = 0.5 - 4\,\mathrm{kg\,m^{-3}s^{-1}}$ [30–32], $p_{met} = 1\,\mathrm{kW\,m^{-3}}$ [39] and $\sigma_t = 0.33\ \Omega^{-1}\mathrm{m}^{-1}$ (a 100 kHz) [40]. They are within the range of values typically quoted for the human tissues. Moreover, a spatially uniform distribution of MNPs in the tumour has been assumed. This is by no means restrictive, as the thermal regime outside D_1 is essentially dependent on the total amount of MNPs.

The values assumed for the physical parameters of the MNPs are those of magnetite nanoparticles (Fe_3O_4 NP, later on). We consider Fe_3O_4 NPs due to their high biocompatibility and non toxicity. In particular, as far as Equation 11 is concerned, the following values have been adopted for the involved parameters: $M_s \approx 318\,\mathrm{kA\,m^{-1}}$, $\tau_0 \approx 10^9\,\mathrm{s}$ and $k_a \approx 15\,\mathrm{kJ\,m^{-3}}$ [41]. Moreover, to compute τ_B an effective viscosity, η, of about $1.6 \times 10^{-2}\,\mathrm{N\,s\,m^{-2}}$ has been set, which is about 16 times larger than the viscosity of pure water [42]. This augmented value of η takes into account not only the viscosity of the medium containing the MNPs, but also the presence of the coating layer which increases the hydrodynamic volume of each MNP. As far as Equation 13 is concerned, the following values have been assumed for the involved parameters: $\alpha = 5 \times 10^{-3}\,\mathrm{J\,m^{-1}\,A^{-3}}$, $\mu_0 M_R = 0.125\,\mathrm{T}$, $H_M = 35\,\mathrm{kA\,m^{-1}}$ and $d_1 = 15\,\mathrm{nm}$. They are the value experimentally found by Hergt et al. [9] for wet chemically grown Fe_3O_4 NPs of 30 nm in size.

Concerning the characteristics of the applied field, a uniform, z-directed MF has been assumed:

$$\underline{H}(\underline{r}) = H\mathrm{rect}\left(\frac{z}{2L}\right)\hat{i}_z \tag{15}$$

where $\hat{i}_z$ is the unit vector along the z axis (see Figure 1A), z is the axial coordinate, L is the half length of the irradiated region and rect $(\cdot)$ is the rectangular window function. The sharp truncation of the exposure region is clearly unrealistic from a physical point of view, but does not affect significantly the results of the analysis, due to the smoothing characteristics of the diffusion operator in Equation 1, while significantly simplifies the mathematics.

From Equation 15 and according to Faraday's law, the following EF has been used in the calculation:

$$\underline{E}(\underline{r}) = (-i\mu_0 H f \pi r)\mathrm{rect}\left(\frac{z}{2L}\right)\hat{i}_\varphi \tag{16}$$

where i is the imaginary unit and $\hat{i}_\varphi$ is the unit vector along the azimuthal direction.

The above assumptions allow exploitation of spherical and cylindrical harmonics for representing the temperature field, thus enabling the solving analytically of Equation 1 by means of a mode matching technique.

Finally, concerning the requirements of hyperthermia and heating selectivity, the analysis has been carried out by setting $T_1 = 42^{\circ}\mathrm{C}$ (mild hyperthermia), $T_2 = 39^{\circ}\mathrm{C}$, $T_{\mathrm{ext}} = T_0{}^{\circ}\mathrm{C}$ and assuming the spherical shape for the transition region surrounding the tumour, with a radius R_2 depending on the value of the tumour radius R_1.

Table I. Numerical results obtained from the proposed criterion.

w_b (kg m^{-3} s^{-1})	r (cm)	R_1 (cm)	R_2 (cm)	$R(L)$ (cm)	p_m (kW m^{-3})	p_e (kW m^{-3})	Hf (Am^{-1}s^{-1})	T_{max} (°C)	Case
0.5	0	1	2	15 (10)	131	3.12	3.14×10^8	45.36	1
	0	1	2	10 (7)	131	1.87	3.67×10^8	45.32	2
	0	0.75	1.5	7.5 (5)	213	0.36	2.13×10^8	45.16	3
	0	0.75	1.5	5 (5)	213	1.02	5.40×10^8	45.15	4
1	0	1	2	15 (10)	175	7.40	4.86×10^8	46.14	5
	0	1	2	10 (7)	170	7.44	7.28×10^8	46	6
	0	0.75	1.5	7.5 (5)	242	9.02	1.07×10^9	45.42	7
	0	0.75	1.5	5 (5)	242	6.43	1.35×10^9	45.41	8
2	0	1	2	15 (10)	238	11.18	5.95×10^8	46.96	9
	0	1	2	10 (7)	235	13.17	9.69×10^8	46.82	10
	0	0.75	1.5	7.5 (5)	324	15.31	1.39×10^9	46.19	11
	0	0.75	1.5	5 (5)	304	19.62	2.37×10^9	45.92	12
4	0	1	2	15 (10)	344	20.83	8.12×10^8	47.85	13
	0	1	2	10 (7)	342	23.60	1.30×10^9	47.71	14
	0	0.75	1.5	7.5 (5)	447	26.47	1.83×10^9	47.02	15
	0	0.75	1.5	5 (5)	433	32.54	3.05×10^9	46.85	16
1	0.5	1	2	5 (5)	158	6.82	1.39×10^9	45.89	17
	1	1	2	5 (5)	157	6.88	1.40×10^9	45.99	18
	1.5	1	2	5 (5)	154	7.31	1.44×10^9	45.92	19

Later, for the reader's convenience, we will present and discuss separately the results obtained for p_m, p_e and Hf from those obtained for H_o, f_o, d_o and c.

Results relative to p_m, p_e and Hf

The results obtained for p_m, p_e and Hf from the numerical analysis as well as the values assumed for w_b, r, R_1, R_2, R, and L, representing the analysed cases, are summarised in Table I. For comparison, in Table I we have also reported, for each case, the maximum value (T_{max}) reached by the induced temperature field T. In all cases, T_{max} is reached inside the tumour.

The analysis has been performed assuming different values of the blood perfusion rate, namely $w_b = 0.5,\ 1,\ 2,\ 4\,\mathrm{kg\,m^{-3}\,s^{-1}}$. Moreover, for each of them, four different values of R_1, R_2, R, L have been considered. The aim has been to investigate the influence of the blood perfusion rate and tumour size and depth on the estimates of p_m, p_e and Hf.

To test the criterion under different conditions we have also distinguished between tumour-centred (i.e. cases 1–16) and not centred (i.e. cases 17–19) on the z axis.

From the achieved results one can note that the estimated values of Hf significantly depend on the dimensions and on the blood perfusion rate of the irradiated region. In particular, as was expected, Hf increases by decreasing R and by increasing w_b. Moreover, except for cases 1, 2, and 3 ($w_b = 0.5\,\mathrm{kg\,m^{-3}\,s^{-1}}$), the obtained values of Hf are larger than the safety threshold $4.85 \times 10^8\ \mathrm{Am^{-1}\,s^{-1}}$, usually adopted in literature. Accordingly, our calculation indicates that this constraint in most cases underestimates the actual range of values of H and f exploitable in MNPH and so the possibility of reducing the therapeutic concentration of MNPs.

On the contrary, in all the considered cases Hf is appreciably smaller than the empirical value 5×10^9 $\mathrm{Am^{-1}s^{-1}}$ used in the estimations performed by Hergt and Dutz [15]. Therefore, according to our results, this value is too large for a safe and selective anticancer treatment by means of MNPH.

It must be stressed that, besides the estimation of the product Hf, the application of the proposed criterion also allows evaluation of the magnetic power level to be dissipated in the tumour to meet the therapeutic requirement of hyperthermia and heating selectivity. Therefore, one can estimate the actual dosage of MNPs to be supplied, given the features of the MNPs to be used in the treatment.

The temperature distribution obtained over the irradiated tissues for some of the cases reported in Table I, namely cases 3, 16 and 19, are shown in Figure 2A–F. In particular, Figure 2A–C show the isothermal curves (solid grey lines) of the produced temperature field, in the plane x–z. The dashed circles delimit the malignant and the surrounding transition regions. On the other side, the curves shown in Figure 2D–E represent the radial profiles, in the plane $z = 0$ of the temperature field obtained for cases 3 and 16, respectively, i.e. when $r = 0$ (tumour centred on the z axis), while the solid grey lines in Figure 2F are the isothermal curves, in the plane $z = 0$ ($z = 0$ is the axial coordinate of the centre of the tumour) of the temperature field obtained for case 19, i.e. when $r \neq 0$ (tumour not centred on the z axis). As can be seen in all cases, the obtained temperature distribution satisfies the assigned

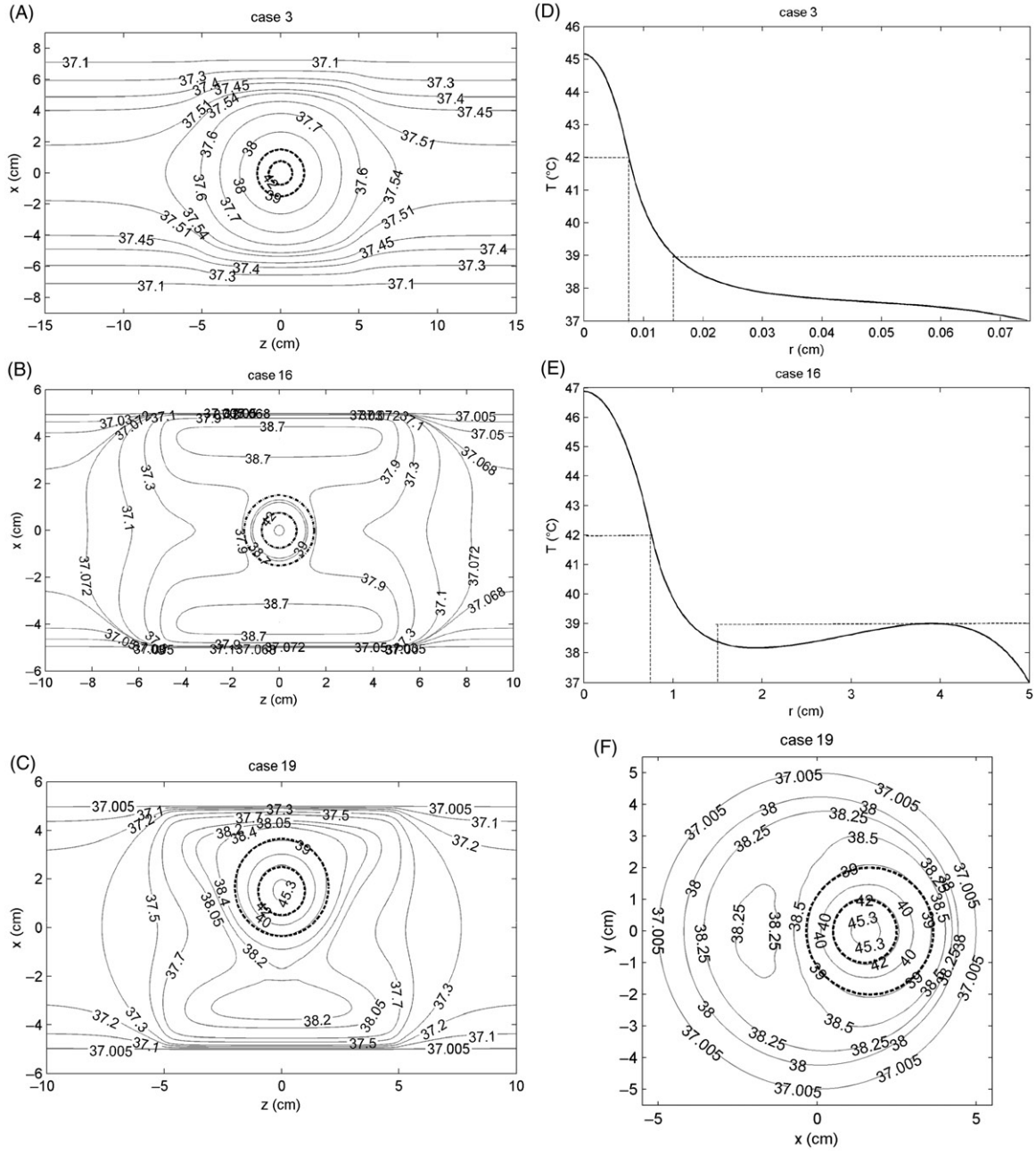

Figure 2. Temperature distribution produced over the irradiated tissues for cases 3 (A and D), 16 (B and E) and 19 (C and F) reported in Table I. (A–C) Distribution in the plane x–z; (D–E) radial profile in the plane $z = 0$ for cases 3 and 16, respectively; (F) distribution in the plane $z = 0$ for case 19.

requirements of hyperthermia and heating selectivity. Moreover, no overheating is observed within the transition region. The obtained results prove the reliability of the proposed criterion and show that its application allows control of the temperature rise produced over the irradiated tissues, avoiding useless and harmful overheating and heat-spot generation in the healthy tissues, thus assuring a safe treatment.

As a concluding remark, let us note that for $w_b = 4\,\mathrm{kg\,m^{-3}\,s^{-1}}$, i.e. case 16, a transition region narrower than the desired one and a very large value of T_{max} ($\approx 47^{\circ}$C) has been obtained (see Figure 2B, 2E and Table I). The observed behaviour can be easily explained by noting that for high values of w_b the perfusion term in Equation 1 becomes dominant as compared to the conductive term, thus the corresponding temperature field becomes practically proportional to the heat generation term $\dot{q}(\underline{r})$. Consequently, the temperature rise produced inside and immediately outside the tumour is practically due to the only magnetic power dissipated by the MNPs in the tumour, being $p_m \gg p_e$. That results in a

Table II. Optimal values for H, f, d obtained from the value of p_m, p_e reported in Table I (i.e. cases 3, 7, 16 and 19). For MF amplitudes above 20 kA m^{-1} Equation 11 is assumed no longer valid.

Case	H_{max} (kA m^{-1})	H_o (kA m^{-1})	f_o (kHz)	d_o (Eq. 11)* (nm)	d_o (Eq. 13) (nm)	c_{min} (Eq. 11)* (mg mL^{-1})	c_{min} (Eq. 13) (mg mL^{-1})	σ_d
3	10	10	21.3	20.5 (22–17)	9.5	16.9 (13.8–30.1)	28.6	0.15
7	10	10	106.9	17.5 (19.3–14.5)	9.5	6.5 (4.5–11.3)	6.5	0.15
7	10	10	106.9	17 (19.2–14)	10.5	3.3 (2.3–6)	4.4	0.05
7	10	10	106.9	18.5 (20–16.3)	9.5	10.6 (7.7–16.4)	10	0.3
7	15	15	71.3	18 (19.8–15)	11	4 (2.3–6.6)	6.2	0.15
7	20	20	53.5	18 (20.2–15.6)	12	2.8 (2–4.34)	5.3	0.15
7	35	35	30.6	–	28	–	4	0.15
7	40	40	26.7	–	21	–	3.9	0.15
7	45	40	26.7	–	21	–	3.9	0.15
16	15	15	203.1	16.5 (18.7–13.8)	11	2.9 (2–5.3)	3.9	0.15
19	15	15	96.2	17.5 (19.4–14.6)	11	2 (1.4–3.4)	2.9	0.15

*The values in brackets are estimated by assuming $k_a = 10$–30 kJ/m^3.

higher degree of heating selectivity of the treatment as shown in Figure 2B and 2E, but also in a higher value of p_m to be dissipated for achieving the therapeutic temperature increase, as confirmed by the values of p_m reported in Table I and relative to $w_b = 4$ kg m^{-3} s^{-1}.

Results relative to H_o, f_o, d_o and c

The values of H_o, f_o and d_o as well as the corresponding values of c, namely c_{min}, estimated for cases 3, 7, 16 and 19 in Table I, are summarised in Table II. For the sake of comparison, we report the results achieved by exploiting both Equations 11 and 13.

Moreover, the estimates have been performed by considering different values for H_{max} and for the standard deviation, σ_d, of the MNP size distribution $g_d(\rho|\mu_d, \sigma_d)$, here assumed lognormal (see Table II). Obviously, the estimated values of d_o represent the mean value of the MNP size distribution, i.e. μ_d.

As can be seen from Table II, as long as H_{max} is smaller than 1.43 $H_{cmax} \approx 41$ kA m^{-1} ($H_{cmax} \approx 29$ kA m^{-1} for wet chemically grown Fe_3O_4 NPs of 30 nm in size [9]), H_{max} represents the optimal value for the MF amplitude also when Equation 13 is used as expression of p_m (see rows 5–9 in Table II).

Concerning c_{min}, its value decreases either by reducing the degree of polydispersivity of the MNPs (see rows 2–4 in Table II) or by increasing the MF amplitude (see rows 5–8 in Table II). The first result is a consequence of the presence in the MNP sample of a higher fraction of MNPs having size close to the optimal one; the second is in agreement with the fact that c is a decreasing function of H (see Appendixes A and B). The optimal MNP diameters obtained by using Equation 11 lie essentially in the range 16–20 nm, in agreement with the experimental data reported in [5, 21, 22].

To show the robustness of the criterion against the uncertainty of the value of k_a, in Table II (in brackets) we have also reported the values of d_o and c_{min} estimated by varying k_a over the range 10–30 kJ/m^3. The obtained results show that c_{min} increases at most linearly with increasing k_a. This proves the robustness of the proposed criterion and the consistency of the obtained estimates on the minimum MNP concentration required for a safe and effective treatment of cancer.

Finally, let us note that, except for case 1, where a very low blood perfusion rate has been assumed, values of c_{min} not larger than about 10 mg of MNP per mL of tumour have been obtained. In particular, values of c_{min} even smaller than about 3 mg/mL have been obtained as long as sufficiently monodisperse MNPs (see row 3 in Table II), moderate perfused tissues (see rows 6 and 10 in Table II) and/or suitable MF amplitudes (see rows 6 and 8 in Table II) are involved. These values, about 3 to 4 times smaller than those typically quoted in literature for the treatment of tumour of comparable sizes [1, 2, 15], suggest that the application of the proposed criterion could significantly improve the MNPH performances.

On the limits of clinical scalability of MNPH

In this section, by exploiting the presented criterion, we will analyse the limits of clinical scalability of MNPH.

Since they are related to the maximum concentration, say c_{lim}, of MNPs reachable in the tumour, their estimation has been performed according to the following steps:

- by evaluating for a suitable set of values of R_1 and R, the minimum concentration, c_{min}, required for achieving the therapeutic heating of the tumour with the desired degree of selectivity (this task is accomplished by exploiting the proposed criterion);

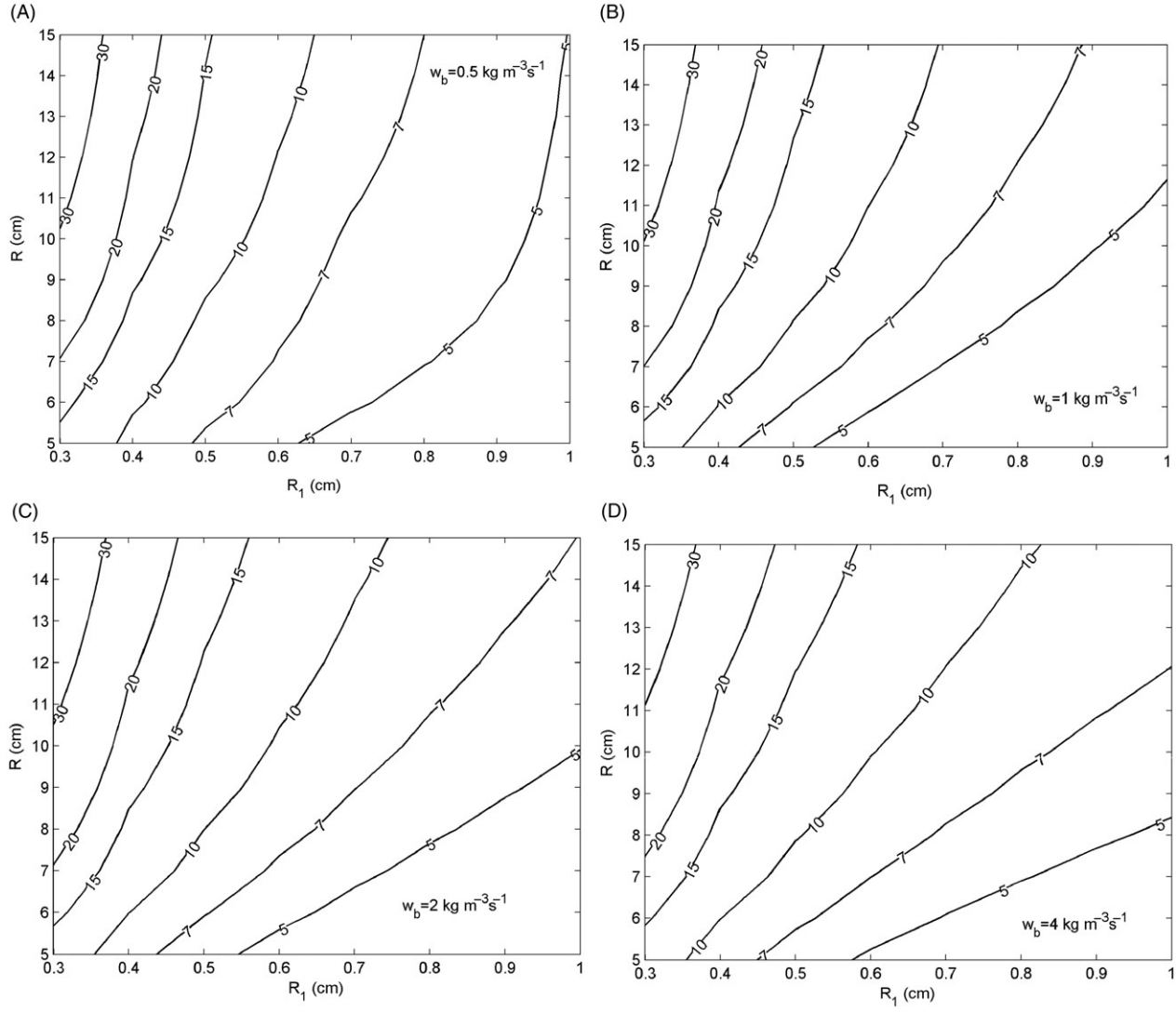

Figure 3. Contour plot of the behaviour of $c_{\min}$ versus the radius of the tumour, R_1, and the radius of the surrounding irradiated tissue, R, for different value of the blood perfusion rate: (A) $w_b = 0.5\,\mathrm{kg\,m^{-3}\,s^{-1}}$; (B) $w_b = 1\,\mathrm{kg\,m^{-3}\,s^{-1}}$; (C) $w_b = 2\,\mathrm{kg\,m^{-3}\,s^{-1}}$; (D) $w_b = 4\,\mathrm{kg\,m^{-3}\,s^{-1}}$.

- by comparing the values obtained for $c_{\min}$ to c_{lim} and considering the values of R_1 and R for which $c_{\min} \leq c_{lim}$.

The analysis has been carried out by again assuming tumours of spherical shape embedded in tissues of cylindrical geometry. In particular, the radius of the tumour, R_1, is varied over the range 3–10 mm, while the radius of the surrounding irradiated tissue, R, is varied over the range 5–15 cm. Moreover, for each value of R_1 a transition region width, $R_2 = R_1 + 10$ mm, has been considered. Clearly, the values assumed for R_1 and R are consistent with the tumour sizes typically detectable by means of conventional diagnostic techniques as well as with the typical dimensions of the various parts of the human body (arms, legs, torso, neck, etc.) that could be involved in the treatment.

The values adopted for the electric and thermal properties of the tissues, as well as the requirements of hyperthermia and heating selectivity are the same assumed in the numerical analysis performed in the previous section. The values assumed for the physical parameters of the MNPs are those typically quoted for Fe_3O_4 NPs size, i.e. $M_s \approx 318\,\mathrm{kA\,m^{-1}}$, $\tau_0 \approx 10^{-9}\,\mathrm{s}$ and $k_a \approx 15\,\mathrm{kJ\,m^{-3}}$. Furthermore, a MF amplitude of $15\,\mathrm{kA\,m^{-1}}$ and a lognormal distribution for the Fe_3O_4 NPs, with a standard deviation $\sigma_d = 0.2$, have been used too. These values are in agreement with those typically quoted in literature [1, 2].

Figure 3A–D show the behaviour of $c_{\min}$ for different values of the blood perfusion rate, i.e. $w_b = 0.5$, 1, 2 and $4\,\mathrm{kg\,m^{-3}\,s^{-1}}$, respectively (each curve is parameterised to a different value of $c_{\min}$). For the sake of brevity, we report only the results obtained by using Equation (11).

From each figure it can be noted that $c_{\min}$ decreases with R_1 and increases with R, in full agreement with the behaviour expected for c. Therefore, related to c_{lim}, there exist lower and upper limits for the size of the tumour and the surrounding irradiated tissue, beyond which tumours cannot be safely and effectively treated by MNPH. These limits can be graphically estimated by drawing on each Figure 3A–D the curve $c_{\min} = c_{lim}$ and considering the values of R_1 and R associated to its end points. Obviously, the sizes of the tumour and the irradiated tissue safely and effectively treatable in MNPH are those associated to the points on the right side of the curve $c_{\min} = c_{lim}$.

By assuming for c_{lim} a value of 10 mg/mL (this value is the typical concentration achievable in the tumour by means of intratumoural injection [1, 2, 15]), our calculations show that, for $w_b = 0.5\,\mathrm{kg\,m^{-3}\,s^{-1}}$ (see Figure 3A), the minimum tumour radius successfully treatable is about 4 mm, as long as an exposed region with a radius not larger than 5 cm is involved. For tumours of increasing size the extension allowed for the surrounding irradiated region increases, and for malignancies with a radius larger than about 6.5 mm no limit exists on the width of the irradiated region, at least within the range of values here assumed for R.

For higher values of w_b, one can note that smaller values for the minimum tumour size effectively treatable are obtained ($R_1 \approx 3.5$ mm for $w_b \geq 1\,\mathrm{kg\,m^{-3}\,s^{-1}}$). However, a reduction of the area of the region on the right side of the curve $c_{\min} = c_{lim}$, resulting in a smaller number of cases treatable, is observed too (see Figure 3A–D). Accordingly, for highly perfused tissues our calculation shows an improvement of the performances of MNPH for tumours not deeply sited in the body (legs, arms, neck, etc.) as well as a worsening for tumours more deeply sited in the body. This apparent contradiction can be explained by noting that for highly perfused tissues the temperature rise inside and immediately around the tumour practically depends only on p_m, especially when a deeply sited tumour is treated. This results in a higher degree of heating selectivity, as clearly shown in Figure 2B and 2E, but at the same time, in a higher value of p_m to be dissipated, and so in a large amount of MNPs to be supplied, for achieving the desired temperature rise.

Accordingly, from the above calculation one can state that, exploiting currently available Fe_3O_4 NPs and concentrations not higher than 10 mg/mL, MNPH is unable to treat malignancies with radius smaller than about 3.5 mm. For tumours of increasing size, the success of the treatment depends on the extension of the tissues to be irradiated, and so on the depth of the malignancy in the body. In particular, the larger the tumour size, the larger the extension allowed for the irradiated region. For malignancies with a radius larger than about 8 mm no limit exists on the width of the irradiated region.

The analysis also shows that the treatment of malignancies smaller than 3 mm in radius or less is possible provided that concentrations of Fe_3O_4 NPs larger than about 15 mg/mL are reached (see Figure 3A–D) within the diseased region. For instance, to successfully treat tumours of 3 mm in radius located at the centre of a tissue with a radius of about 10 cm, a concentration of Fe_3O_4 NPs of approximately 30 mg/mL is needed (see Figure 3A–D). However, this concentration could be reduced again below 10 mg/mL by exploiting MNPs magnetically more efficient than the Fe_3O_4 NPs [43]. According to Equation 11, this result could be achieved by using MNPs with a higher saturation magnetisation, M_s, not larger than twice that of Fe_3O_4 NPs.

The above conclusions are drawn by assuming the MNPs are contained only in the tumoural region. However, by enlarging the portion of tissues targeted by the MNPs beyond the cancerous area, it would be possible to effectively treat tumours smaller than 3 mm in radius, obviously, provided a lower degree of heating selectivity is accepted. Accordingly, apart from the obvious increasing MNP concentration and/or their SAR, a third way is practicable to extend the limits of clinical scalability of MNPH: to enlarge the portion of tissue targeted by the MNPs beyond the cancerous tissue.

Conclusions

A criterion for the individuation of the exposure conditions and the MNP features that minimise the therapeutic concentration of MNPs to be used in MNPH has been presented.

The proposed criterion is based on the estimation of the mean specific heat generation rates, due to the magnetic and electric fields, to be supplied to both the cancerous and surrounding irradiated tissues for achieving the therapeutic heating of the tumour with a desired degree of hyperthermia and selectivity.

The proposed criterion here presented by exploiting the BHTE to describe the temperature rise produced over the irradiated region can be applied whatever the adopted bioheat transfer model provided that a linear description for the heat transfer mechanisms within the involved tissues can be assumed.

The results of an exhaustive numerical analysis performed by assuming electrically and thermally homogeneous tissues prove the reliability of the criterion and show that its application assures a complete and preliminary control of the temperature rise overall the irradiated area, thus avoiding useless

and harmful overheating of the healthy tissues and hence assuring a safe and effective treatment.

Concerning the estimation of the MF characteristics, the obtained results show that in the most of cases the allowable values of *Hf* are larger than the safety threshold 4.85×10^8 $Am^{-1}s^{-1}$, usually considered in the literature. Accordingly, our calculation indicates that in most cases a weaker constraint on the product *Hf* can be considered.

Concerning the estimation of the MNP characteristics, the obtained results show that except for very low perfused tissues concentrations of Fe_3O_4 NPs not larger than 10 mg/mL are sufficient to meet the assigned requirements of hyperthermia and heating selectivity. In particular, concentrations even smaller than about 3 mg/mL have been obtained as long as sufficiently monodisperse Fe_3O_4 NPs, moderately perfused tissues and/or suitable MF amplitudes are involved. These values, about 3–4 times smaller than those typically quoted in the literature for the treatment of tumours of comparable sizes, suggest that the application of the proposed criterion could significantly improve the MNPH performances.

The robustness of the proposed criterion against the uncertainty affecting the values of the MNP parameters has also been assessed. The obtained result further confirms the consistency of the obtained estimates.

Finally, by exploiting the proposed criterion a study of the clinical scalability of the therapeutic approach has also been performed.

The obtained results show that for typical concentrations of available Fe_3O_4 NPs which can be reached today ($\approx$10 mg/mL) MNPH is unable to treat malignancies with a radius smaller than about 3.5 mm. For tumours of increasing size, the success of the treatment depends on the extension of the tissues to be irradiated, i.e. on the depth of the malignancy in the body. In particular, the larger the tumour size, the larger the extension allowed for the irradiated region. The treatment of deeply sited tumours in the body, such as the torso, is also possible provided that the tumours are not too small and suitably perfused tissues are involved.

Possible ways of decreasing the minimum size of treatable tumours have been also briefly discussed.

Future development on this topic will include the application of the criterion to transient regime, the numerical validation of the criterion in the case of electrically and thermally inhomogeneous tissues, the study of the influence of the boundary condition on the estimation of p_m, p_e, and hence on the optimal values of the MF and MNP parameters and on the limits of clinical scalability. Experimental validation of the criterion on phantom models could be also worthwhile.

Acknowledgements

This work has been partially sponsored by the Italian Ministry of University and Research. The authors thank Enrico Bucci for his support and valuable suggestions.

Declaration of interest: The authors report no conflicts of interest. The authors alone are responsible for the content and writing of the paper.

Note

1. Equations 7a and 7b assure the achievement of the temperature requirements within the regions D_1 and $D \backslash D_2$, but say nothing of the transition region, $D_2 \backslash D_1$, wherein the temperature, in principle, could reach any value. However, as long as $p_m \gg p_e$, as it is expected in MNPH, no overheating can occur in the healthy tissue surrounding the tumour.

References

1. Pankhurst QA, Connolly J, Jones SK, Dobson J. Applications of magnetic nanoparticles in biomedicine. J Phys D: Appl Phys 2003;36:R167–R181.
2. Leslie-Pelecky DL, Labhasetwar V, Kraus RH. Nanobiomagnetics. In: Sellmyer DJ, Skomski, and R, editors. Advanced magnetic nanostructures. New York: Springer; 2006. pp 461–490.
3. Thiesen B, Jordan A. Clinical applications of magnetic nanoparticles for hyperthermia. Int J Hyperthermia 2008; 24:467–474.
4. Jordan A, Scholz R, Wust P, Fahling H, Felix R. Magnetic fluid hyperthermia (MFH): cancer treatment with AC magnetic field induced excitation of biocompatible superparamagnetic nanoparticles. J Magn Magn Mater 1999; 201:413–419.
5. Gazeau F, Lévy M, Wilhelm C. Optimizing magnetic nanoparticle design for nonothermotherapy. Nanomedicine 2008;3:831–844.
6. Barry SE. Challenges in the development of magnetic particles for therapeutic applications. Int J Hyperthermia 2008;24: 451–466.
7. Jordan A, Scholz R, Maier-Hauff K, Johannsen M, Wust P, Nadobny J, Schirra H, Schmidt H, Deger S, Loening SA, et al. Presentation of a new magnetic field therapy system for the treatment of human solid tumors with magnetic fluid hyperthermia. J Magn Magn Mater 2001;225:118–126.
8. Rosensweig RE. Heating magnetic fluid with alternating magnetic field. J Magn Magn Mater 2002;252:370–374.
9. Hergt R, Dutz S, Roder M. Effect of size distribution on hysteresis losses of magnetic nanoparticles for hyperthermia. J Phys: Condens Matter 2008;20:1–12.
10. DeNardo SJ, DeNardo GL, Natarajan A, Miers LA, Foreman AR, Gruettner C, Adamson GN, Ivkov R. Thermal dosimetry predictive of efficacy of 111In-ChL6 nanoparticle AMF-induced thermoablative therapy for human breast cancer in mice. J Nucl Med 2007;48:437–444.
11. Johannsen M, Gneveckow U, Eckelt L, Feussner A, Waldofner N, Scholz R, Deger S, Wust P, Loening SA, Jordan A. Clinical hyperthermia of prostate cancer using magnetic nanoparticles: Presentation of a new interstitial technique. Int J Hyperthermia 2005;21:1–11.
12. Johannsen M, Gneveckow U, Taymoorian K, Thiesen B, Waldöfner N, Scholz R, Jung K, Jordan A, Wust P,

Loening SA. Morbidity and quality of life during thermotherapy using magnetic nanoparticles in locally recurrent prostate cancer: Results of a prospective phase I trial. Int J Hyperthermia 2007;23:315–323.
13. Hildebrandt B, Schoeler D, Ringel F, Kerner T, Wust P, Riess H, Schriever F. Differential gene expression in peripheral blood lymphocytes of cancer patients treated with whole body hyperthermia and chemotherapy: A pilot study. Int J Hyperthermia 2006;22:625–635.
14. Atsarkin VA, Levkin LV, Posvyanskiy VS, Melnikov OV, Markelova MN, Gorbenko OY, Kaul AR. Solution to the bioheat equation for hyperthermia with $La_{1-x}Ag_yMnO_{3-\delta}$ nanoparticles: The effect of temperature autostabilization. Int J Hyperthermia 2009;25:240–247.
15. Hergt R, Dutz S. Magnetic particle hyperthermia – Biophysical limitations of a visionary tumour therapy. J Magn Magn Mater 2007;311:187–192.
16. Brusentsov NA, Gogosov V, Brusentsova TN, Sergeev AV, Jurchenko NY, Kuznetsov AA, Kuznetsov OA, Shumakov LI. Evaluation of ferromagnetic fluids and suspensions for the site-specific radiofrequency-induced hyperthermia of MX11 sarcoma cells in vitro. J Magn Magn Mater 2001;225: 113–117.
17. Jordan A, Wust P, Scholz R, Tesche B, Fähling H, Mitrovics T, Vogl T, Cervós-navarro J, Felix R. Cellular uptake of magnetic fluid particles and their effects on human adenocarcinoma cells exposed to AC magnetic fields in vitro. Int J Hyperthermia 1996;12:705–722.
18. Zhai Y, Xie H, Gu H. Effects of hyperthermia with dextran magnetic fluid on the growth of grafted H22 tumour in mice. Int J Hyperthermia 2009;25:65–71.
19. Jordan A, Maier-Hauff K. Magnetic nanoparticles for intracranial thermotherapy. J Nanosci Nanotechnol 2007; 7:4604–4606.
20. Wust P, Gneveckow U, Johannsen M, Böhmer D, Henkel T, Kahmann F, Sehouli J, Felix R, Ricke J, Jordan A. Magnetic nanoparticles for interstitial thermotherapy – Feasibility, tolerance and achieved temperatures. Int J Hyperthermia 2006;22:673–685.
21. Hergt R, Dutz S, Muller R, Zeisberger M. Magnetic particle hyperthermia: Nanoparticle magnetism and materials development for cancer therapy. J Phys: Condens Matter 2006;18:S2919–S2934.
22. Glockl G, Hergt R, Zeisberger M, Dutz S, Nagel S, Weitschies W. The effect of field parameters, nanoparticle properties and immobilization on the specific heating power in magnetic particle hyperthermia. J Phys: Condens Matter 2006;18:S2935–S2949.
23. Brezovich IA. Low frequency hyperthermia. Med Phys Monograph 1988;16:82–111.
24. Arkin H, Xu LX, Holmes KR. Recent developments in modeling heat transfer in blood perfused tissues. IEEE Trans Biomed Eng 1994;41:97–107.
25. Lv YG, Deng ZS, Liu J. 3-D numerical study on the induced heating effects of embedded micro/nanoparticles on human body subject to external medical electromagnetic field. IEEE Trans Nanobioscience 2005;4:284–294.
26. Bagaria HG, Johnson DT. Transient solution to the bioheat equation and optimization for magnetic fluid hyperthermia treatment. Int J Hyperthermia 2005;21:57–75.
27. Salloum M, Ma R, Zhu L. An in vivo experimental study of temperature elevations in animal tissue during magnetic nanoparticle hyperthermia. Int J of Hyperthermia 2008; 24:589–601.
28. Pavel M, Gradinariu G, Stancu A. Study of the optimum dose of ferromagnetic nanoparticles suitable for cancer therapy using MFH. IEEE Trans Magn 2008;44:3205–3208.
29. Zhang C, Johnson DT, Brazel CS. Numerical study on the multi-region bio-heat equation to model magnetic fluid hyperthermia (MFH) using low Curie temperature nanoparticles. IEEE Trans Nanobioscience 2008;7:267–275.
30. Lang J, Erdmann B, Seebass M. Impact of nonlinear heat transfer on temperature control in regional hyperthermia. IEEE Trans Biomed Eng 1999;46:1129–1138.
31. Kowalski ME, Jin JM. Model-based optimization of phased arrays for electromagnetic hyperthermia. IEEE Trans Microwave Theory Tech 2004;52:1964–1977.
32. Candeo A, Dughiero F. Numerical FEM models for the planning of magnetic induction hyperthermia treatments with nanoparticles. IEEE Trans Magn 2009;45:1658–1661.
33. Severens NMW, Van Marken Lichtenbelt WD, Frijns AJH, Van Steenhoven AA, De Mol BAJM, Sessler DI. A model to predict patient temperature during cardiac surgery. Phys Med Biol 2007;52:5131–5145.
34. Rai KN, Rai SK. Effect of metabolic heat generation and blood perfusion on the heat transfer in the tissues with a blood vessel. Heat Mass Trans 1999;35:75–79.
35. Fortin JP, Wilhelm C, Servais J, Ménager C, Bacri JC, Gazeau F. Size-sorted anionic iron oxide nanomagnets as colloidal mediators for magnetic hyperthermia. J Am Chem Soc 2007;129:2628–2635.
36. Gonzales-Weimuller M, Zeisberger M, Krishnan KM. Size-dependent heating rates of iron oxide nanoparticles for magnetic fluid hyperthermia. J Magn Magn Mater 2009; 321:1947–1950.
37. Skumiel A, Jòzefczak A, Hornowski T. Investigation of magnetic and hyperthermic effects in ferrofluids with PEG biocompatible surfactant. J Phys: Conference Series 2009;149:1–4.
38. Fujita S, Tamazawa M, Kuroda K. Effects of blood perfusion rate on the optimization of RF-capacitive hyperthermia. IEEE Trans Biomed Eng 1998;45:1182–1186.
39. Muffin MD, St Jeor ST, Hill LA, Scott BJ, Daugherty SA, Koh YO. A new predictive equation for resting energy expenditure in healthy individuals. J Clin Nutr 1990; 51:241–247.
40. Gabriel C. Dielectric properties of biological materials. In: Barnes, FS, and Greenebaum B, editors. Bioengineering and Biophysical Aspects of Electromagnetic Fields. CRC Press; 2006. pp 52–100.
41. Malaescu I, Marin CN. Study of magnetic fluids by means of magnetic spectroscopy. Physica B 2005;365:134–140.
42. Bicknese S, Periasamy N, Shohet SB, Verkman AS. Cytoplasmic viscosity near the cell plasma membrane: Measurement by evanescent field frequency-domain microfluorimetry. Biophys J 1993;65:1272–1282.
43. Kline TL, Xu YH, Jing Y, Wang JP. Biocompatible high-moment FeCo-Au magnetic nanoparticles for magnetic hyperthermia treatment optimization. J Magn Magn Mater 2009;321:1525–1528.

Appendix A: Optimal choice for H, f, d by adopting Equation 11 as expression of p_m

We will show that $H_o = H_{\max}$ when Equation 11 is the expression adopted for p_m. To this end, let us note that from Equation 11 one has:

$$c = \frac{9k_bTp_m}{\pi(\pi\mu_0 M_s Hf)^2}\frac{1+\left(2\pi f\tau_{eff}(d)\right)^2}{\tau_{eff}(d)d^3} \qquad \text{(A1)}$$

Then, by combining Equation A1 and Equation 10 one gets:

$$c = a\frac{1 + b\left(2\pi\tau_{eff}(d)/H\right)^2}{\tau_{eff}(d)d^3} = c(H, d) \qquad \text{(A2)}$$

where a and b are constant quantities having the following expressions:

$$a = \frac{9}{2}\frac{p_m}{p_e}\frac{k_b T\bar{\sigma}_t}{\pi(\pi M_s)^2} \qquad \text{(A.3)}$$

$$b = \frac{2p_e}{\mu_0^2\bar{\sigma}_t} \qquad \text{(A.4)}$$

From Equation A2 one can easily note that c, as a function of H, decreases monotonically. As a result, whatever the value assumed for d, c reaches the minimum for $H = H_{\max}$. Thus, $H_o = H_{\max}$. Obviously, the corresponding value of d_o is obtained by minimising the right hand of Equation A2 with $H = H_o$, which is equivalent to maximising the right hand of Equation 11.

It is worth noting that Equation 11 holds for monodisperse MNPs. When polydisperse MNPs are considered, the right hand of Equation 11 has to be weighted according to the particle-size distribution $g_d(\rho|\mu_d, \sigma_d)$. Therefore, the obtained result could not be applicable in the more realistic case of polydisperse MNPs.

Actually, at least in the case of a lognormal size distribution with usual standard deviations, it keeps still valid. As a matter of fact, a numerical analysis shows that, whatever the value of μ_d, c remains a decreasing function of H. Thus, we have again $H_o = H_{\max}$.

Appendix B: Optimal choice for H, f, d by adopting Equation 13 as expression of p_m

We will show that $H_o = \min\{H_{\max}, 1.43H_{c\max}\}$ as long as Equation 13 is the expression adopted for p_m. To this end, by setting $x = H_c(d)/H$ in Equation 13 one has:

$$p_m = ca\left((x - x^6)u(1 - x) + \frac{\alpha H^2}{4\mu_0 M_R}d(x)u(x - 1)\right) \qquad \text{(B1)}$$

where $a = 4\mu_0 M_R Hf$ is a constant quantity ($Hf \propto p_e$) and the dependence of d on x follows from the equation $x = H_c(d)/H$.

It can be easily proven that the first term in brackets on the right hand of Equation B1 reaches the maximum for $x = \sqrt[5]{1/6}$, independently of the value assumed for d, while the second term reaches the maximum when $H = H_{c\max}$ and $x = 1$, i.e., when $d(x) = d_{\max}$ (see Equation 14). Since the maximum value of the first term ($\sim$0.58) is larger than that of the second term ($\sim$0.16 for wet chemically grown Fe_3O_4 NPs of 30 nm in size [9]), the maximum of p_m is assumed for $x = \sqrt[5]{1/6}$ namely when $H_o = \sqrt[5]{6}\,H_c(d) \approx 1.43\ H_c(d)$, independently of the value assumed for d. Then, a possible choice for H_o and d_o is: $H_o = 1.43H_{c\max}$ and $d = d_{\max}$.

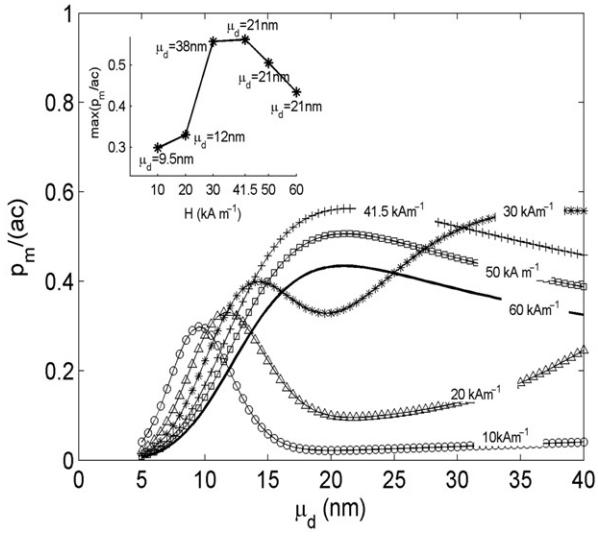

Figure 4. Behaviour of p_m/ac ($a = 4\mu_0 M_R Hf$) versus μ_d estimated by using Equation 13 as expression of p_m and in the case of polydisperse MNPs. A lognormal distribution, with $\sigma_d = 0.2$, has been assumed. Each curve is relative to a different value of H. The inset reports the maximum values assumed by each curve in figure, versus H and the corresponding values of μ_d.

It is worth noting that the obtained result holds for monodisperse MNPs. When polydisperse MNPs are considered, the right hand of Equation B1 has to be weighted according to the particle-size distribution $g_d(\rho|\mu_d, \sigma_d)$ or, equivalently, with the distribution $g_x(\rho|\mu_x, \sigma_x)$, obtained from $g_d(\rho|\mu_d, \sigma_d)$ according to the transformation $x = H_c(d)/H$, ($H_c(d)$ is given by Equation 14). Therefore, the obtained result may not be applicable in the more realistic case of polydisperse MNPs.

Again, it stays valid in the case of a lognormal size distribution, as shown by the numerical results shown in Figure 4. Here the behaviour of p_m/ac vs μ_d, for different values of the MF amplitude H and for a standard deviation $\sigma_d = 0.2$, has been reported. The inset displays the maximum values assumed by each curve versus H together with corresponding values of μ_d. As can be seen, the largest value of p_m/ac, i.e. the largest value of SAR (SAR $= (a/\rho_m)\ p_m/ac$ where a/ρ_m is a constant, being ρ_m the mass density of the MNPs), is reached for $H = 41.5\,\text{kA m}^{-1} \approx 1.43H_{c\max}$ and $\mu_d = 21\,\text{nm} \approx d_{\max}$. Also, for $H < 1.43H_{c\max}$ $\max\{p_m/ac\}$ is an increasing function of H. As a consequence $H_o = \min\{H_{\max}, 1.43H_{c\max}\}$, where $H_{\max}$ is the maximum MF amplitude that the used exposure apparatus can produce.